The ER membrane protein complex is important for the biogenesis of flavivirus polyproteins

Ashley M Ngo[1], Matthew J Shurtleff[2], Katerina D Popova[2], Jessie Kulsuptrakul[1], Jonathan S Weissman[2,3], Andreas S Puschnik[1,4]

[1] Chan Zuckerberg Biohub, San Francisco, United States

[2] Department of Cellular and Molecular Pharmacology, University of California, San Francisco, San Francisco, United States

[3] Howard Hughes Medical Institute, University of California, San Francisco, San Francisco, United States

[4] Correspondence to: andreas.puschnik@czbiohub.org

Abstract

Flaviviruses such as dengue (DENV), Zika (ZIKV) or West Nile virus (WNV) translate their genome as a single multi-pass transmembrane (TM) protein at the endoplasmic reticulum (ER) membrane. Several genetic knockout (KO) screens identified the ER membrane protein complex (EMC) as a critical host component for flavivirus infection. The EMC facilitates accurate insertion, topology and/or stabilization of specific cellular TM proteins including a subset of tail-anchored proteins and G protein-coupled receptors. Here, we show that deletion of EMC in human cell lines decreased infection with DENV, ZIKV and WNV by 100 to 10,000-fold. Using replicon studies and immunoblotting in EMC KO cells, we demonstrated that the EMC was essential for viral protein expression. Ribosome profiling of DENV-infected wild-type and EMC KO cells revealed no drastic differences in translation efficiency. Instead, we found that a large fraction of expressed viral proteins was targeted to the proteasome post-translationally. In order to identify regions of the viral polyprotein that depend on the EMC for proper folding and stability, we used two orthogonal approaches: First, we generated a dual fluorescence-based reporter fused to different segments

27 of the viral polyprotein and detected a decrease in stability in NS4A-NS4B, a region rich in
28 transmembrane domains. Second, we performed iterative passaging of DENV on EMC KO cells
29 and identified non-synonymous point mutations in NS4A and NS4B. Introduction of adapted
30 mutations rescued both viral replication and stable expression of the NS4A-4B polyprotein
31 segment. Lastly, we showed a physical interaction between the EMC and DENV NS4B protein
32 post-cleavage and rapid degradation of processed NS4B in the absence of EMC. Together, our
33 results suggest that the EMC engages with DENV polyproteins to ensure proper biogenesis of
34 the NS4A-4B region. Thus, our data elucidates how flaviviruses hijack the EMC and provides
35 further evidence for the cellular function of the EMC in the stable expression of TM proteins.
36

37 **Introduction**

38 Flaviviruses such as dengue (DENV), Zika (ZIKV) or West Nile virus (WNV) express their genome
39 as a single multi-pass transmembrane (TM) protein at the endoplasmic reticulum (ER) membrane.
40 Subsequently, the polyprotein is cleaved by the viral NS2B-NS3 protease and the cellular signal
41 peptidase into the individual structural (C, prM, E) and non-structural (NS1-5) proteins required
42 for replication and assembly into new virions (reviewed in Neufeldt et al., 2018). Similar to cellular
43 TM proteins, the viral polyprotein relies on the host cell machinery for targeting to the ER,
44 translocation across the membrane and insertion of transmembrane domains (TMDs) into the
45 lipid bilayer during its translation. These processes are facilitated by the signal recognition particle
46 (SRP), the translocon-associated protein (TRAP) complex (also known as signal-sequence
47 receptor complex), the Sec61 translocon and the signal peptidase complex. These cell
48 components were all identified as essential host factors for flavivirus infection in genetic screens
49 underscoring their importance for virus replication (Krishnan et al., 2008; Marceau et al., 2016;
50 Sessions et al., 2009; Zhang et al., 2016). For most TM proteins, recognition of a hydrophobic
51 TMD or signal sequence by the SRP followed by transfer to the Sec61 translocation channel are
52 sufficient for membrane targeting and accurate topogenesis (Shao and Hegde, 2011). Recently,

53 it was shown that the ER membrane protein complex (EMC) plays a role in the insertion and/or
54 stabilization of certain TM proteins (Chitwood et al., 2018; Guna et al., 2018; Shurtleff et al., 2018).
55 Intriguingly, several genome-wide CRISPR knockout (KO) screens for flavivirus dependency
56 factors showed strong enrichment of the EMC (Ma et al., 2015; Marceau et al., 2016; Savidis et
57 al., 2016; Zhang et al., 2016). However, its role in the virus life cycle is not yet understood.
58 The EMC was discovered in a genetic screen for yeast mutants modulating the unfolded protein
59 response (UPR) (Jonikas et al., 2009). Genetic interaction mapping and biochemical purification
60 revealed a six-subunit core complex (EMC1-6) conserved in yeast and mammals (Christianson
61 et al., 2011; Jonikas et al., 2009). Other than its more general association with UPR and ER-
62 associated degradation (ERAD), the EMC was shown to interact co-translationally and enable
63 biogenesis of a subset of multi-pass TM proteins (Shurtleff et al., 2018). Biochemical
64 characterization of select EMC-dependent TM proteins, such as tail-anchored proteins and G
65 protein-coupled receptors (GPCRs), revealed that the EMC is capable of inserting TMDs into the
66 ER membrane (Chitwood et al., 2018; Guna et al., 2018).
67 Here, we investigated how the mosquito-borne flaviviruses, DENV, ZIKV and WNV, depend on
68 the EMC during infection. We showed that the EMC was required for DENV polyprotein
69 biogenesis and identified a segment spanning NS4A-4B as the region dependent on the EMC for
70 stable expression. Absence of the EMC resulted in post-translational degradation of viral proteins.
71 Together, our data highlights how flaviviruses hijack important machinery for TM protein
72 biogenesis to achieve optimal expression of their polyproteins, which reinforces a role for the EMC
73 in stabilizing challenging TM proteins during synthesis.
74
75 **Results**
76 To validate the enrichment of the EMC components in the flavivirus CRISPR screens, we
77 generated isogenic EMC subunit KO cell lines in Huh7.5.1 and HEK293FT, two cell types that
78 were used for the genetic screens (Figure S1A). Upon infection with DENV expressing Renilla

79 luciferase (DENV-Luc), we measured a ~10,000-fold reduction in viral replication in Huh7.5.1
80 EMC1-6 KO cells (Figure 1A) and a 10-1,000-fold reduction in HEK293FT EMC1-5 KO cells
81 (Figure 1B). The differences in the extent of the phenotypes may be attributed to the presence of
82 compensatory pathways or the degree of disruption of the entire protein complex between the
83 two cell types upon knockout of a single subunit. The strong deficit in DENV replication in the
84 absence of the EMC persisted over a 30-72h period (Figure S1B). Complementation of EMC2
85 and EMC4 KO cells with the respective cDNA completely restored levels of DENV infection
86 (Figures 1C and S1C). Lastly, we tested the effect of EMC4 KO on several flaviviruses and saw
87 a significant decrease of viral RNA for DENV, WNV and ZIKV but not hepatitis C virus (HCV),
88 which is a more distantly related member of the *Flaviviridae* family (Figures 1D and S1D). This is
89 congruent with results of an HCV CRISPR screen that did not identify the EMC as a critical host
90 factor (Marceau et al., 2016). This finding highlights that there is a specific, evolutionarily
91 conserved dependency on the EMC among mosquito-borne flaviviruses and not a universal
92 disruption of trafficking to and/or translation or replication at the ER membrane, which would affect
93 a wider range of viruses.
94
95 Next, we sought to determine at which step of the viral life cycle the EMC is required. As the EMC
96 is important for the expression of a large set of TM proteins, its disruption leads to an altered cell
97 surface proteome, which may affect viral entry. We measured effects on viral uptake in WT and
98 EMC4 KO cells by quantifying the amount of internalized viral RNA at 2 and 6 hours post-infection
99 (hpi), where we did not observe a difference (Figure 2A). Only at 24hpi, a timepoint when viral
100 replication had occurred, was a difference in RNA load evident between WT and EMC4 KO cells.
101 Furthermore, we used a DENV replicon expressing luciferase, which bypasses entry and does
102 not produce viral particles, thus allowing the analysis of the effect of EMC KO specifically on
103 translation and replication. In this assay, we saw decreased luminescence in EMC4 KO cells
104 starting at 12 hours post-electroporation suggesting that the EMC is important during or prior to

105 viral replication (Figure 2B). We additionally performed the replicon assay in the presence of MK-
106 0608, a nucleoside analogue that inhibits the viral polymerase (Chen et al., 2015), and observed
107 that the luminescence signal in EMC4 KO cells was lower than in replication-inhibited WT cells
108 suggesting that deletion of EMC has an effect on viral translation, which happens prior to
109 replication (Figure S2A). To further dissect effects on translation or genome replication of DENV,
110 we conducted an immunoblot timecourse series, where WT and EMC4 KO cells were infected at
111 a high multiplicity of infection (moi=32) and lysates were harvested at early timepoints post-
112 infection (6-12hpi), when no or only little DENV replication had occurred. Viral protein expression
113 was lower in EMC4 KO compared to WT cells as early as 6hpi further supporting a translation
114 defect (Figures 2C and S2B). To rule out any contribution of low levels of replication to the
115 observed phenotype, we also performed the immunoblot experiment in the presence of MK-0608
116 and still saw different amounts of DENV protein accumulation between WT and EMC4 KO cells
117 indicating that the EMC is indeed important for viral protein expression (Figures S2C and S2D).
118 Interestingly, while the EMC has been implicated in the stable biogenesis of TM proteins, we
119 found reduced expression of both TMD and non-TMD containing viral proteins. This suggests that
120 the defect likely occurs at the polyprotein stage thus affecting all individual, cleaved proteins.
121
122 The expression of flaviviral proteins is a complex process that requires several steps. DENV
123 translation is initiated in a cap-dependent manner, whereupon the single-stranded positive-sense
124 RNA genome is translated into a single ~3,400 amino acid long multi-pass TM protein. This
125 polyprotein is co- and post-translationally processed by host and viral proteases producing the
126 individual functionally active structural and non-structural proteins. We first tested whether the
127 defect occurs at the stage of polyprotein translation. We used ribosome profiling, which captures
128 the average number of ribosomes on a given mRNA species with positional information, to
129 compare translation efficiencies (TE) and successful full-length synthesis of both cellular and viral
130 proteins in WT and EMC4 KO cells (Ingolia et al., 2009). Thus, any changes in TE or premature

131 ribosome stalling in EMC KO vs WT cells would be reflected by changes in ribosomal footprints
132 (as measured by Ribo-seq) normalized to changes in mRNA abundance (as measured by RNA-
133 seq). In the uninfected condition, we did not observe dramatic changes in TE for cellular mRNAs
134 in EMC4 KO vs WT cells (Figure 3A and Supplementary Table 1). This is in line with previously
135 reported results using CRISPRi knockdown against EMC subunits suggesting that deletion of
136 EMC does not largely affect the synthesis rates of its client proteins (Shurtleff et al., 2018).
137 Similarly, we did not find any substantial differences in viral TE in EMC4 KO cells relative to WT
138 cells at 18 (0.43x) and 44hpi (2.17x) (Figures 3B and 3C and Supplementary Table 1). Rather we
139 observed that DENV RNA was among the highest translated (top 0.1%) mRNAs in both WT and
140 EMC4 KO cells (Figure S3A). The lower number of ribosomal footprints aligning to the viral
141 genome in EMC4 KO cells was largely due to the reduced number of viral RNA copies present in
142 the cells. Moreover, footprints were able to be mapped throughout the viral genome in EMC4 KO
143 cells, which suggests that synthesis of full-length polyprotein still occurred (Figure S3B).
144 Therefore, we concluded that translation of DENV polyproteins is not drastically affected, which
145 led us to explore potential post-translational defects.
146 Proper insertion of TMDs and correct folding are required for stable expression of TM proteins,
147 while misfolded proteins are targeted to the proteasome for degradation via the ERAD pathway.
148 To probe whether an increased fraction of viral proteins is sent for degradation in EMC deficient
149 cells, we infected WT and EMC4 KO cells with DENV in the presence of Bortezomib (BZ), a
150 proteasome inhibitor, thus preventing removal of misfolded proteins from the cells. Indeed, BZ
151 treatment led to an increase of detectable viral proteins in EMC4 KO cells but not WT cells (Figure
152 3D). Addition of BZ, however, did not restore DENV replication confirming that the proteasome-
153 targeted proteins are non-functional (Figure S3C). Together, this suggests that in the absence of
154 EMC viral proteins are still translated but are unable to achieve a stable conformation resulting in
155 their degradation and inability to establish efficient replication.
156

157 For cellular multi-pass client proteins, such as transporters and GPCRs, the EMC co-
158 translationally engages with specific TMDs in order to support insertion into the membrane and
159 allow stable expression of the entire TM protein (Chitwood et al., 2018; Shurtleff et al., 2018). We
160 used two orthogonal methods, a fluorescence-based protein stability assay and viral evolution, to
161 examine which region of the viral polyprotein requires the EMC for successful expression. First,
162 we utilized a dual-color fluorescent reporter as previously described (Chitwood et al., 2018). The
163 C terminus of different segments of the DENV polyprotein was fused to eGFP followed by a viral
164 T2A sequence and mCherry (G2C) (Figure 4A). Translation of the fusion constructs generates
165 two protein products at a 1:1 ratio due to peptide bond skipping by the ribosome at the T2A site:
166 1) a polyprotein segment fused to eGFP and 2) mCherry. Any post-translational instability of the
167 eGFP fusion protein due to misfolding results in an eGFP:mCherry ratio of less than 1. As
168 expected, the cytosolic G2C-only construct displayed a 1:1 ratio in both WT and EMC4 KO cells,
169 while the β_1-adrenergic receptor (ADRB1) fused to G2C exhibited drastic destabilization in EMC4
170 KO compared to WT cells as was previously reported (Figure 4B) (Chitwood et al., 2018). Applying
171 this approach to different DENV polyprotein G2C fusion constructs, we observed that the
172 segments containing only the structural proteins (capsid, prM and E) or NS1-3 were not
173 destabilized in EMC4 KO Huh7.5.1 cells (Figure 4B). By contrast, constructs encoding both NS4A
174 and NS4B (but not either of them alone) showed reduced stability in EMC4 KO cells (Figure 4B).
175 Similar results were obtained in HEK293FT (Figure S4). NS4A has 3 TMDs with the third (termed
176 2K peptide) being highly hydrophobic and serving as a signal sequence for the translocation of
177 NS4B into the ER membrane (Lin et al., 1993). Subsequently, the NS4A-2K junction is cleaved
178 by the viral protease and the 2K-NS4B junction by the signal peptidase. As the 2K-targeted NS4B-
179 5-G2C construct did not display a stability defect in EMC deficient cells, the results suggest that
180 EMC mediates stable expression by first engaging within NS4A prior to the 2K peptide and that a
181 defect in NS4A topogenesis is extended to the NS4B region.

182 Stability of NS4A-4B-G2C was restored to near WT levels by complementation of EMC4 KO cells
183 with EMC4 cDNA (Figure 4C). Moreover, treatment of EMC4 KO cells with BZ increased the
184 eGFP:mCherry ratio of NS4A-4B-G2C in EMC4 KO cells indicating that this region of the
185 polyprotein is misfolded and targeted for degradation in the absence of EMC (Figure 4D).
186 Therefore, we linked the DENV replication phenotype in EMC deficient cells to a specific
187 molecular defect in the NS4A-4B region of the polyprotein.
188
189 In a second, orthogonal approach, we performed viral adaptation to evolve EMC-independent
190 DENV mutants by passaging the virus consecutively on EMC4 KO Huh7.5.1 cells every 3-4 days.
191 After 20-22 passages we observed cell death in 3 out of 6 independent adaptation experiments.
192 Sequencing of RNA extracted from supernatant and alignment to the WT16681 DENV genome
193 revealed two non-synonymous point mutations in NS4A and NS4B, which were conserved across
194 all three isolates (Figure 5A). The A6665G mutation led to a tyrosine to cysteine and the A7558T
195 mutation to an asparagine to tyrosine substitution. The majority of other SNPs was silent (Figure
196 S5A). A6665G is predicted to be inside a TMD helix encoding region of NS4A suggesting that this
197 TMD relies on the EMC for proper ER membrane insertion (Miller et al., 2007). Only one of 1,359
198 DENV serotype 2 genomes from the NCBI database has a G at this position encoding cysteine,
199 while other sequences all encode tyrosine. This evolutionary conservation suggests that this
200 residue indeed has an important function. Similarly, the frequency of A at position 7558 is very
201 conserved with 99.6%, and there is no T encoding tyrosine in the 1,359 sequenced strains.
202 Interestingly, A7558T resides in a non-TMD region at the end of NS4B, thus likely supporting
203 membrane insertion or folding in a different manner (Miller et al., 2006). To demonstrate that the
204 acquired mutations confer independence from EMC, we infected WT and EMC4 KO cells with
205 WT16681 or the three evolved DENV isolates and measured replication. WT16681 DENV
206 displayed a ~100-fold decrease in viral RNA in EMC4 KO relative to WT cells, while the EMC
207 adapted isolates had equal RNA levels (Figure 5B). To dissect whether both mutations are

208 required for optimal replication in EMC KO background, we introduced them individually or in
209 tandem into the DENV-Luc infectious clone and generated virus. While A6665G and A7558T
210 individually restored DENV replication in EMC4 KO cells to 30 and 86% of WT levels, respectively,
211 the double mutant displayed complete rescue of viral growth (Figure 5C). We also introduced the
212 two adapted mutations into NS4A-5-G2C, which showed increased stability in EMC4 KO cells
213 compared to the WT construct thus reverting the molecular destabilization phenotype (Figure 5D).
214 Remarkably, the G2C fluorescence assay and viral adaptation independently pinpointed NS4A-
215 4B of the polyprotein as the region which requires the EMC. The results of the two experiments
216 suggest that a defect in stable insertion of the NS4A TMD2 could lead to subsequent failure in
217 accurate topogenesis of NS4B. By contrast, polyprotein segments starting with 2K-NS4B were
218 stably expressed in EMC KO cells as was shown using NS4B-5-G2C construct (Figure 4A).
219 Therefore, the EMC is required for correct insertion, processing and/or folding of the NS4A-4B
220 region.
221
222 Finally, to probe how absence of EMC causes failure of DENV replication, we transfected a
223 subgenomic NS2B-4B construct (containing functional NS2B-NS3 for polyprotein cleavage) with
224 C terminal fusion to eGFP into WT and EMC4 KO cells and immunoblotted against the different
225 processed products. While there was no notable difference between the higher molecular weight
226 intermediates (NS2B-NS3-NS4A-NS4B-eGFP or NS4A-NS4B-eGFP), we observed reduced
227 accumulation of processed NS4B-eGFP in EMC4 KO cells (Figure 6A). BZ treatment indicated
228 rapid degradation of cleaved NS4B-eGFP in EMC deficient cells. Furthermore, if the EMC acts to
229 insert or stabilize NS4A-4B, we hypothesized that direct binding of NS4B to EMC post polyprotein-
230 processing should be detectable in WT cells. We performed a co-immunoprecipitation using
231 FLAG-tagged EMC4 and detected NS4B but not prM or NS5 in the pulldown (Figure 6B). Overall,
232 this supports the finding that EMC physically engages with NS4A-4B to facilitate its biogenesis
233 and stable expression.

234

235 **Discussion**

236 Based on our results and previous work (reviewed in Chitwood and Hegde, 2019) we propose the
237 following model for the role of the EMC in flavivirus infection. During translation of the polyprotein
238 the EMC engages with TMDs in the NS4A and NS4B region to facilitate their correct insertion into
239 the ER membrane, by which correct topology, processing and stable expression of individual viral
240 proteins are achieved (Figure 6C). In the absence of the EMC, TMDs in the NS4A-NS4B region
241 are not stably or accurately integrated in the ER membrane leading to misfolding and degradation
242 of processed NS4B. NS4A and NS4B fulfill crucial functions for viral replication. NS4A induces
243 ER membrane rearrangements important for the formation of viral replication complexes (Miller
244 et al., 2007; Roosendaal et al., 2006) while NS4B interacts with the NS3 helicase and also
245 suppresses the cellular interferon response (Muñoz-Jordán et al., 2005; Zou et al., 2015). It
246 remains to be studied whether the other viral proteins are destabilized due to an overall topology
247 defect in the NS4A-4B region of the polyprotein or if lack of functional NS4A and/or NS4B inside
248 the replication complexes results in instability of all viral proteins.

249 In addition to characterizing the role of the EMC in the viral life cycle, our data also helps to further
250 elucidate its cellular function. The emerging role of the EMC to facilitate topogenesis has been
251 implicated for several cellular TM proteins (Chitwood et al., 2018; Coelho et al., 2019; Guna et
252 al., 2018; Shurtleff et al., 2018; Volkmar et al., 2019). For a subset of tail-anchored proteins, the
253 EMC inserts the sole C-terminal TMD after translation is completed in the cytosol (Guna et al.,
254 2018). Moreover, the EMC co-translationally inserts the first N-terminal TMD of many GPCRs with
255 an N_{exo} topology (N terminus in the ER lumen) (Chitwood et al., 2018). By contrast, we found
256 EMC-dependency within DENV NS4A-4B, a region with several TMDs, which are not close to the
257 termini of the polyprotein. This provides experimental evidence that the EMC is not only capable
258 of supporting insertion and stable expression of TMDs near the N and C termini but also of internal
259 TMDs. Additionally, it is noteworthy that the DENV polyprotein is distinct from human TM proteins

260 in that it contains multiple signal peptidase cleavage sites along the polyprotein, including at the
261 2K/NS4B site between NS4A and NS4B, which removes the 2K peptide acting as signal sequence
262 for NS4B (Lin et al., 1993; Miller et al., 2006). Interestingly, it was shown (e.g. for ADRB1) that
263 addition of a signal sequence or an N_{cyt} TMD upstream of the first N_{exo} TMD makes the EMC
264 dispensable for biogenesis (Chitwood et al., 2018). This observation suggests that EMC-mediated
265 integration/stabilization may be context-dependent and supports a direct role of the EMC in the
266 stable expression of the wide variety of implicated TM proteins beyond tail-anchored proteins and
267 GPCRs.
268 Generally, for both cellular multi-pass TM proteins and the DENV polyprotein, only one or a subset
269 of TMDs seem to require the EMC for accurate topogenesis, while the other TMDs rely on the
270 Sec61 translocon. The exact interplay between Sec61 and the EMC during TM protein biogenesis
271 warrants further investigation. The simultaneous dependency of flaviviruses on both Sec61 and
272 EMC as highlighted by the CRISPR KO screens could allow an in-depth analysis of the sequence
273 and TMD features that may determine membrane insertion via Sec61 or EMC.
274 The A6665G mutation is predicted to be in a TM helix of NS4A but A7558T is not in a TM region
275 (Miller et al., 2006, 2007). Therefore, further studies are necessary to determine the exact
276 interaction between the EMC and the viral TMDs. Interestingly, the A6665G mutation also arose
277 during DENV adaptation to cell lines deficient in the oligosaccharyltransferase (OST) complex,
278 another critical host factor inside the ER membrane (Marceau et al., 2016; Puschnik et al., 2017).
279 The OST complex has been shown to be important for RNA genome replication in a catalytically
280 independent function and was suggested to act as structural scaffold for viral replication
281 complexes. It is possible that the tyrosine to cysteine substitution generally modulates ER
282 anchoring of NS4A. Overall, it remains to be elucidated how the resulting amino acid substitutions
283 rescue stable expression of NS4A and NS4B.
284 The isolation of EMC-independent DENV mutants additionally enables drug screening for EMC
285 modulators by testing compounds against WT DENV-Luc and then counter-screening hits with

286 EMC-adapted virus. EMC inhibitors may be a useful chemical tool to study EMC function and also
287 provide a potential antiviral therapeutic against flaviviruses. Host-directed antivirals may have the
288 advantage of a broader activity against multiple viruses and a higher barrier of drug resistance.
289 Only 50% of the adaptation experiments yielded escape mutants containing two mutations after
290 >20 passages. For comparison, for direct-acting antivirals (e.g. viral polymerase inhibitors), one
291 point mutation is often sufficient to overcome the mechanism of action (Beaucourt and Vignuzzi,
292 2014).
293 Lastly, the EMC was originally discovered to be associated with the UPR (Jonikas et al., 2009),
294 and upregulation of UPR during flavivirus infection has been reported (Peña and Harris, 2011;
295 Reid et al., 2018; Su et al., 2002). It is possible that competition between viral polyproteins and
296 cellular proteins for the machinery important for proper TM protein expression (such as EMC,
297 OST complex and ERAD components) is linked to this phenomenon. The induction of ER stress
298 can further trigger autophagy, which has also been shown to be beneficial for flavivirus infection
299 (Abernathy et al., 2019; Lee et al., 2018; Senft and Ronai, 2015). Therefore, hijacking the EMC
300 may have direct and indirect implications for flavivirus replication.
301 Overall, our study gives detailed insights into how flaviviruses exploit the EMC to support proper
302 polyprotein expression, and we provide further evidence for the cellular function of the EMC in
303 TM protein topogenesis by utilizing DENV as a cell biological tool.
304

305 **Acknowledgments**

306 We like to thank the following people: Jan Carette for discussions, providing reagents and critically
307 reading the manuscript; Caleb Marceau for technical advice and providing reagents; members of
308 the Biohub Infectious Disease Initiative and the Weissman lab for discussions and technical
309 advice; the Biohub Genomics Platform for help with sequencing. ASP was supported by the Chan
310 Zuckerberg Biohub. MJS is a Howard Hughes Medical Institute Fellow of the Helen Hay Whitney
311 Foundation and JSW is an Investigator of the Howard Hughes Medical Institute.

312

313 **Author contributions**

314 ASP and JSW conceptualized study. AMN and ASP conducted the majority of experiments with

315 help from JK. MJS and KDP performed ribosome profiling. ASP wrote the manuscript with input

316 from all authors.

317

318

319

Figure 1

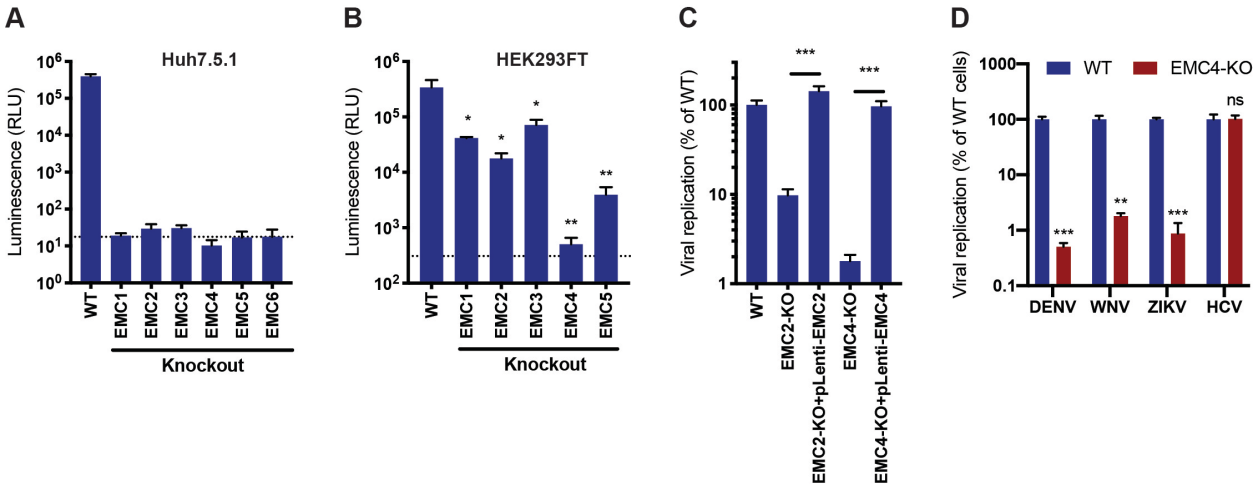

Figure 1: EMC is required for flavivirus infection

(A) Luminescence of WT and EMC subunit KO Huh7.5.1 cells infected with DENV-Luc at 30hpi. Dotted line is background from uninfected control.

(B) Luminescence of WT and EMC subunit KO HEK293FT cells infected with DENV-Luc at 48hpi. Dotted line is background from uninfected control.

(C) Replication of DENV-Luc in WT, EMC2- and EMC4-KO, and cDNA complemented KO HEK293FT cells.

(D) Quantitative RT-PCR of DENV, WNV, ZIKV and HCV RNA in WT or EMC4-KO Huh7.5.1 cells. In all figures, values are shown as mean of three biological replicates with standard deviation in (A)-(C) and mean with standard error of the mean in (D). *t*-tests were performed to determine statistical significance and *p*-values are defined as ns=non-significant, *<0.05, **<0.01, ***<0.001.

Figure 2

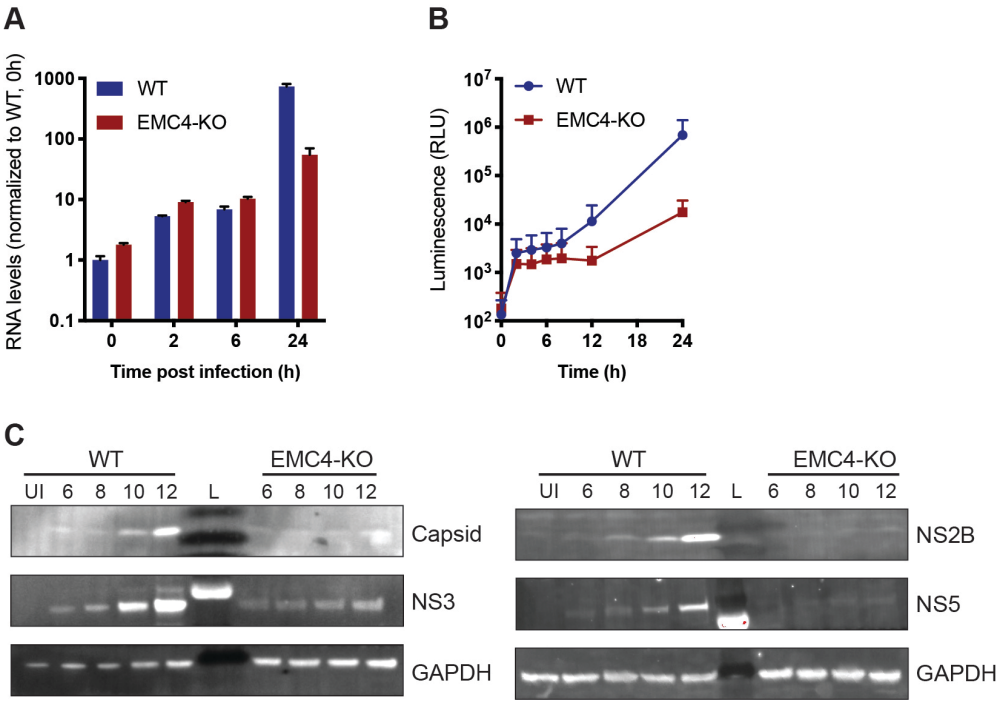

Figure 2: EMC is important for optimal viral protein expression

(A) Quantitative RT-PCR of internalized DENV RNA in WT and EMC4-KO Huh7.5.1 cells at different timepoints post-infection. The data is from three biological replicates and shown as mean with standard error of the mean.

(B) Luminescence of WT and EMC4-KO HEK293FT cells, which were electroporated with DENV replicon expressing Renilla luciferase and collected at different times post-electroporation. The data is from three biological replicates for each timepoint and shown as mean with standard deviation.

(C) Immunoblot analysis of DENV infected WT and EMC4-KO HEK293FT cells at different timepoints post-infection (6/8/10/12h). Lysates were blotted for different viral proteins (Capsid, NS2B, NS3 and NS5) and GAPDH was used as loading control. UI=uninfected control; L=ladder. Quantification of bands is shown in Figure S2B.

Figure 3

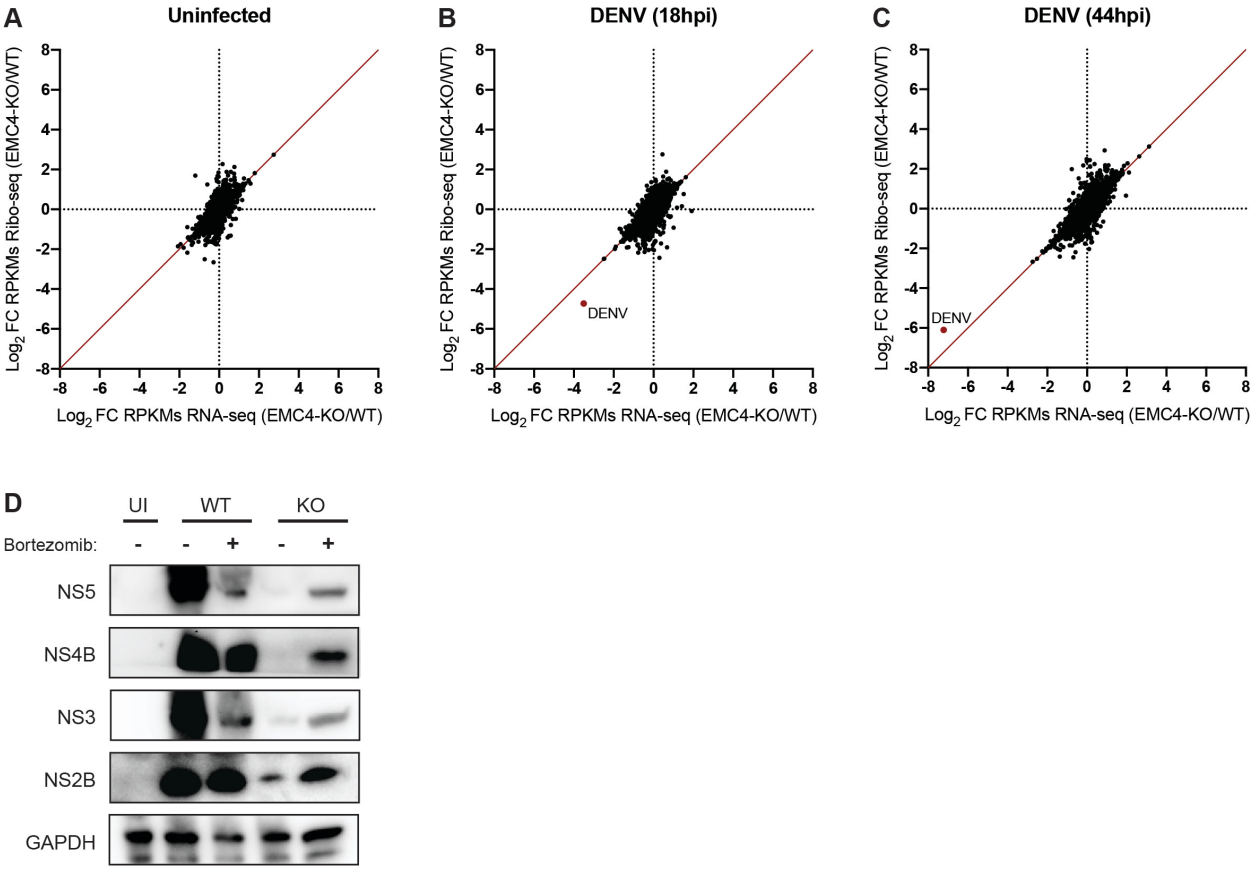

Figure 3: EMC knockout does not largely affect viral translation efficiency but leads to post-translational protein degradation

(A) Ribo-seq and RNA-seq were performed in uninfected WT and EMC4-KO HEK293FT cells to measure changes in translation efficiency (TE). Log_2 fold-change (FC) of reads per kb of transcript, per million mapped reads (RPKMs) between EMC4-KO and WT cells for Ribo-seq and RNA-seq are displayed on the y- and x-axis, respectively. Each dot represents one RNA transcript. Changes in TE for a given transcript is defined as the change in Ribo-seq RPKMs normalized to the change in RNA-seq RPKMs. The red line represents ΔTE=1.

(B) Ribo-seq and RNA-seq were performed in DENV-infected WT and EMC4-KO HEK293FT cells 18h post-infection to measure changes in translation efficiency (TE). The DENV transcript is highlighted in red.

360 (C) Ribo-seq and RNA-seq were performed in DENV-infected WT and EMC4-KO HEK293FT cells
361 44h post-infection to measure changes in translation efficiency (TE). The DENV transcript is
362 highlighted in red.
363 (D) Immunoblot analysis of DENV infected WT and EMC4-KO HEK293FT cells with or without
364 addition of bortezomib (50nM), a proteasome inhibitor at 18hpi. GAPDH was used as loading
365 control. UI=uninfected.
366
367

Figure 4

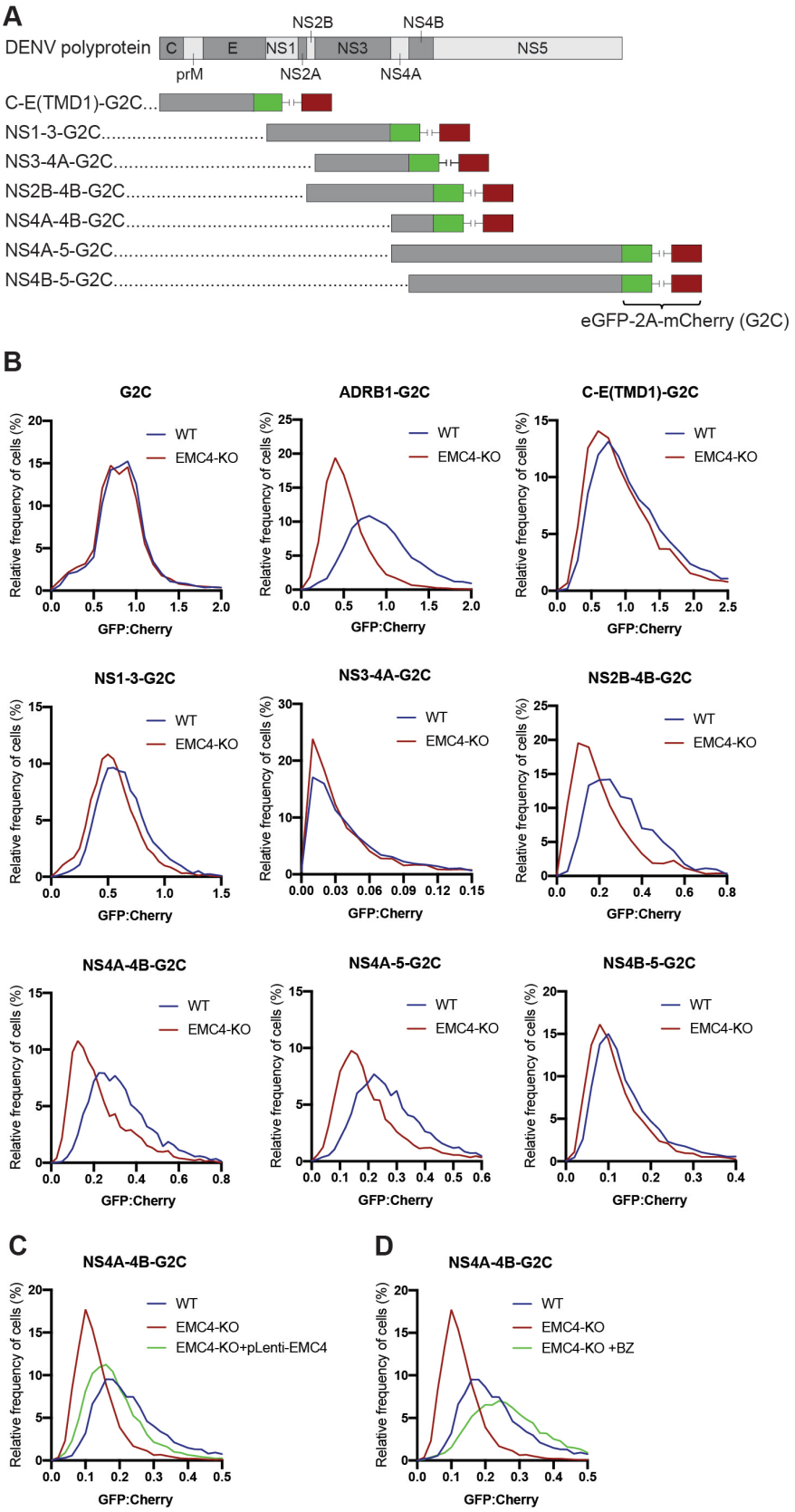
A
DENV polyprotein
C
E
NS1
NS2B
NS3
NS4B
NS5
prM
NS2A
NS4A
C-E(TMD1)-G2C...
NS1-3-G2C.....
NS3-4A-G2C.....
NS2B-4B-G2C.....
NS4A-4B-G2C.....
NS4A-5-G2C.....
NS4B-5-G2C.....
eGFP-2A-mCherry (G2C)
B
G2C
ADRB1-G2C
C-E(TMD1)-G2C
NS1-3-G2C
NS3-4A-G2C
NS2B-4B-G2C
NS4A-4B-G2C
NS4A-5-G2C
NS4B-5-G2C
WT
EMC4-KO
Relative frequency of cells (%)
GFP:Cherry
C
NS4A-4B-G2C
EMC4-KO+pLenti-EMC4
D
EMC4-KO +BZ

368

369 **Figure 4: EMC is required for proper biogenesis of the NS4A-NS4B region of the DENV**
370 **polyprotein**

371 (A) Overview of dual-fluorescence reporter constructs of DENV polyprotein for analysis of protein
372 stability. Segments of the DENV genome encoding parts of the polyprotein were cloned with a C-
373 terminal fusion to eGFP-T2A-mCherry (G2C). The T2A peptide leads to peptide bond skipping
374 during translation resulting in two protein products, DENV protein fused to eGFP and mCherry.
375 The GFP:mCherry fluorescence ratio reflects changes in DENV protein stability.

376 (B) Flow cytometry measurements of GFP:mCherry fluorescence ratio for G2C constructs in WT
377 and EMC4-KO Huh7.5.1 cells. The fluorescence ratios are depicted as histograms. ADRB1=β1-
378 adrenergic receptor.

379 (C) Measurement of GFP:mCherry fluorescence ratio of NS4A-4B-G2C construct in WT, EMC4-
380 KO and EMC4 cDNA complemented EMC4-KO HEK293FT cells.

381 (D) Measurement of GFP:mCherry fluorescence ratio of NS4A-4B-G2C construct in WT, EMC4-
382 KO and bortezomib-treated EMC4-KO HEK293FT cells. Note that (C) and (D) use same WT and
383 EMC4-KO data as experiments were performed in parallel.

384

385

Figure 5

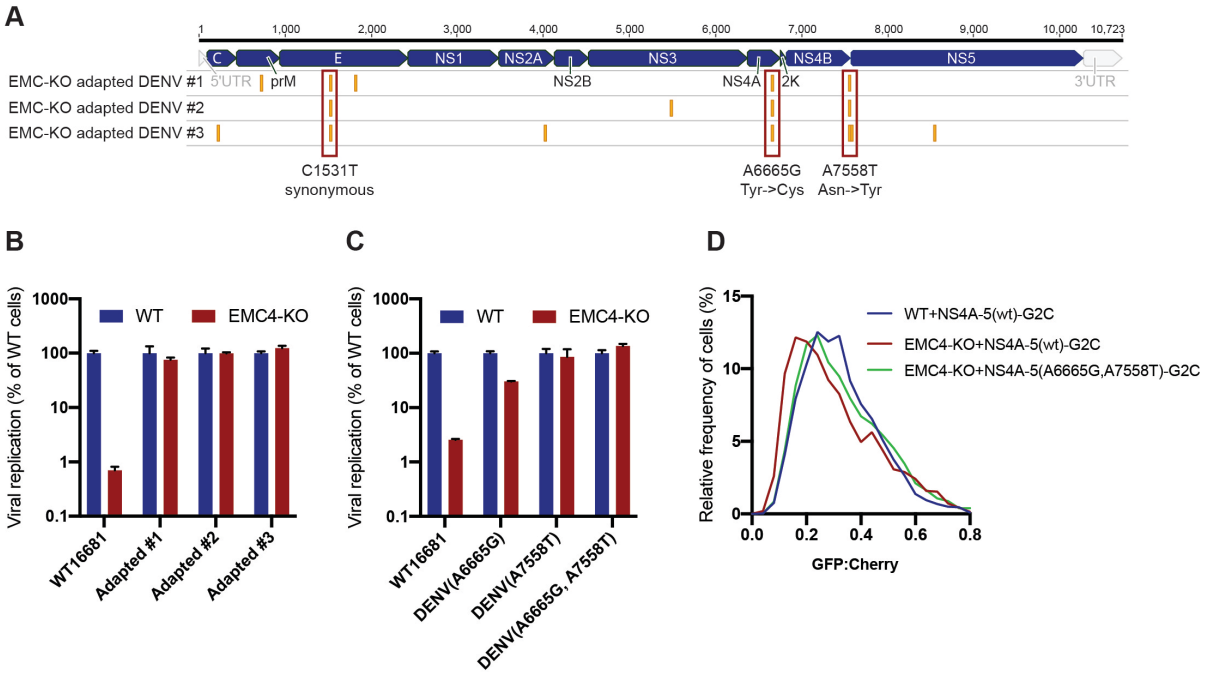

Figure 5: Adaptation of DENV to EMC KO cells reveals non-synonymous point mutations in NS4A and NS4B

(A) Identification of SNPs in EMC4-KO adapted DENV relative to DENV 16681 reference genome by next-generation sequencing of supernatant-extracted viral RNA. Mutations common across all three replicates are highlighted by red boxes and their nucleotide and amino acid changes are shown below. A table of all identified SNPs can be found in Figure S5.

(B) Quantitative RT-PCR of DENV RNA from WT DENV 16681 and the three isolated EMC-adapted DENV in WT and EMC4-KO Huh7.5.1. The data is from three biological replicates and shown as mean with standard error of the mean.

(C) Viral infection assay in WT and EMC4 KO Huh7.5.1 using WT DENV-Luc or mutant DENV-Luc containing A6665G and A7558T either individually or in tandem. The data is from three biological replicates and shown as mean with standard deviation.

(D) Measurement of GFP:mCherry fluorescence ratio of WT NS4A-5-G2C and NS4A-5(A6665G,A7558T)-G2C constructs in WT and EMC4-KO Huh7.5.1.

Figure 6

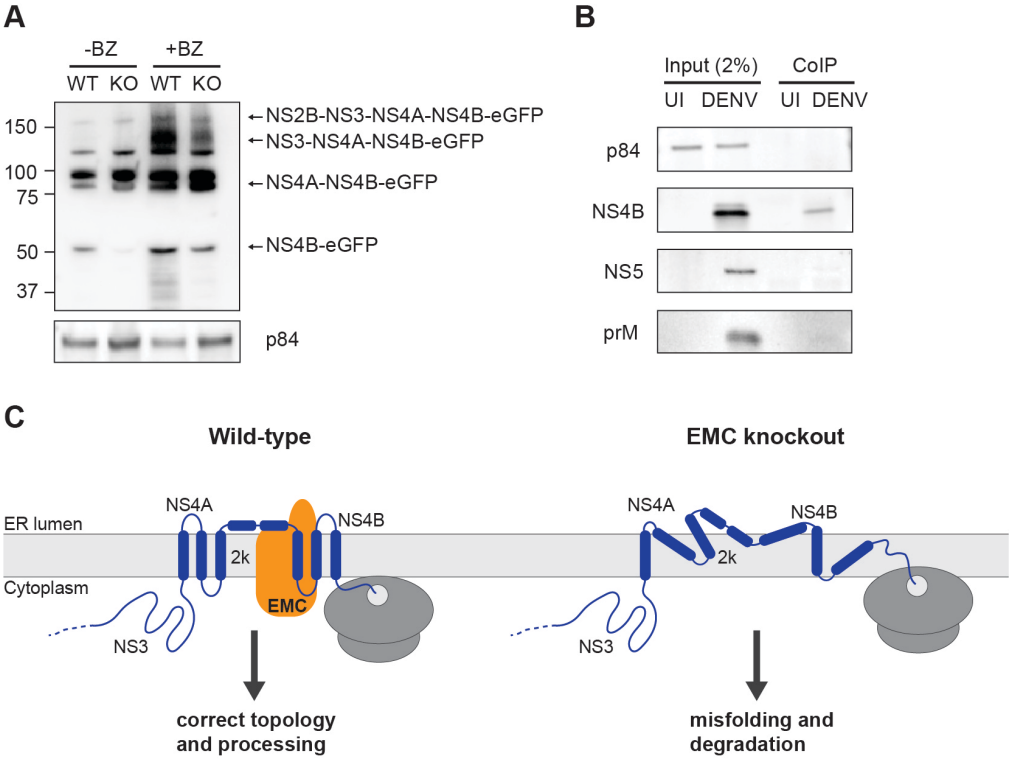

Figure 6.: EMC physically interacts with DENV NS4B post-cleavage and absence of EMC leads to rapid degradation of misfolded NS4B.

(A) Immunoblot for processed products of transfected NS2B-4B-GFP construct in WT and EMC4 KO cells in presence or absence of BZ. p84 was used as loading control.

(B) Co-immunoprecipitation of EMC4-FLAG from lysates of uninfected (UI) or DENV infected HEK293FT EMC4-FLAG cells followed by immunoblotting against viral proteins (prM, NS4B, NS5). p84 was used as loading and non-specific binding control.

(C) Model for the role of EMC in DENV infection. In DENV infected wild-type cells, the EMC co-translationally engages with NS4A and/or NS4B TMDs to facilitate correct/stable insertion ensuring a functional topology. In the absence of the EMC, misfolding of the NS4A-NS4B region occurs during polyprotein synthesis resulting in degradation of viral proteins.

Figure S1

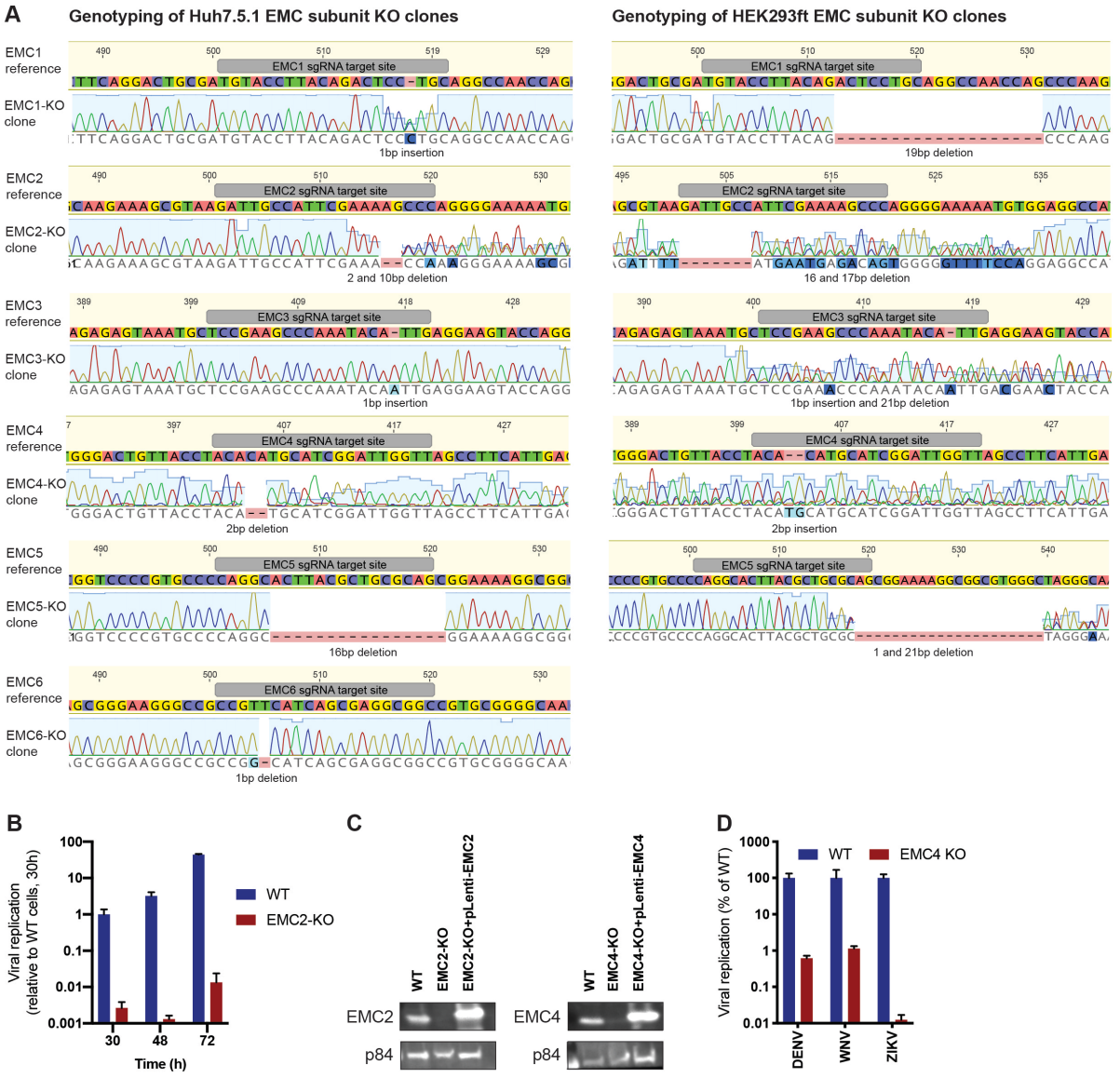

Figure S1: EMC is required for flavivirus infection

(A) Sanger sequencing of clonal EMC subunit KO Huh7.5.1 and HEK293FT cells. sgRNA targeting site is highlighted in reference sequence (top) and indel mutation is shown below sequencing trace of KO cells. For heterozygous mutants, TIDE was used to determine indel mutations.

420 (B) Quantitative RT-PCR of DENV RNA in WT or EMC2-KO Huh7.5.1 at 30, 48 and 72h post
421 infection. Values are shown relative to the WT, 30h condition.
422 (C) Immunoblot analysis of EMC2 or EMC4 expression in WT, EMC2- and EMC4-KO, and cDNA
423 complemented KO HEK293FT cells. p84 was used as loading control.
424 (D) Quantitative RT-PCR of DENV, WNV and ZIKV RNA in WT or EMC4-KO HEK293FT cells.
425 For QPCR experiments, values are shown as mean of three biological replicates with standard
426 error of the mean.
427

Figure S2

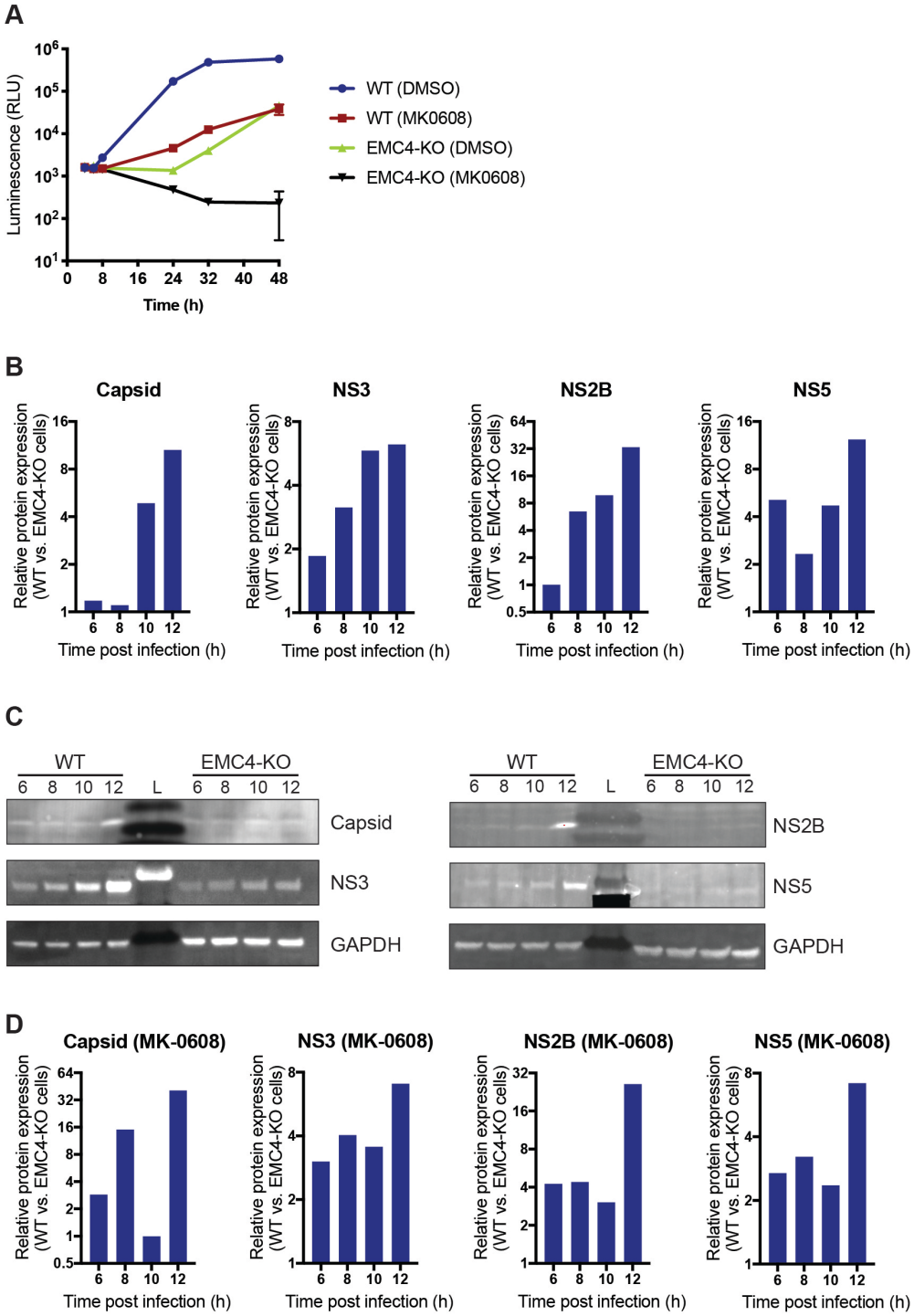

Figure S2: EMC is important for optimal viral protein expression

(A) Luminescence of WT and EMC4-KO cells electroporated with DENV replicon expressing Renilla luciferase and treated with MK-0608 (a nucleoside analogue, which inhibits the DENV

432 polymerase) or DMSO. Lysates were collected at different times post electroporation. The data is
433 from three biological replicates and shown as mean with standard deviation.
434 (B) Quantification of viral protein expression in EMC4-KO cells relative to WT cells by
435 densitometry. Bands of viral proteins from Figure 2C were quantified and normalized to GAPDH
436 bands at each timepoint.
437 (C) Immunoblot analysis of DENV infected WT and EMC4-KO HEK293FT cells at different
438 timepoints post-infection (6/8/10/12h) with treatment of MK-0608 to inhibit viral replication.
439 Lysates were blotted for different viral proteins (Capsid, NS2B, NS3 and NS5) and GAPDH was
440 used as loading control. UI=uninfected control; L=ladder. Quantification of bands is shown in
441 Figure S2D.
442 (D) Quantification of viral protein expression in EMC4-KO cells relative to WT cells by
443 densitometry. Bands of viral proteins from Figure S2C were quantified and normalized to GAPDH
444 bands at each timepoint.
445

Figure S3

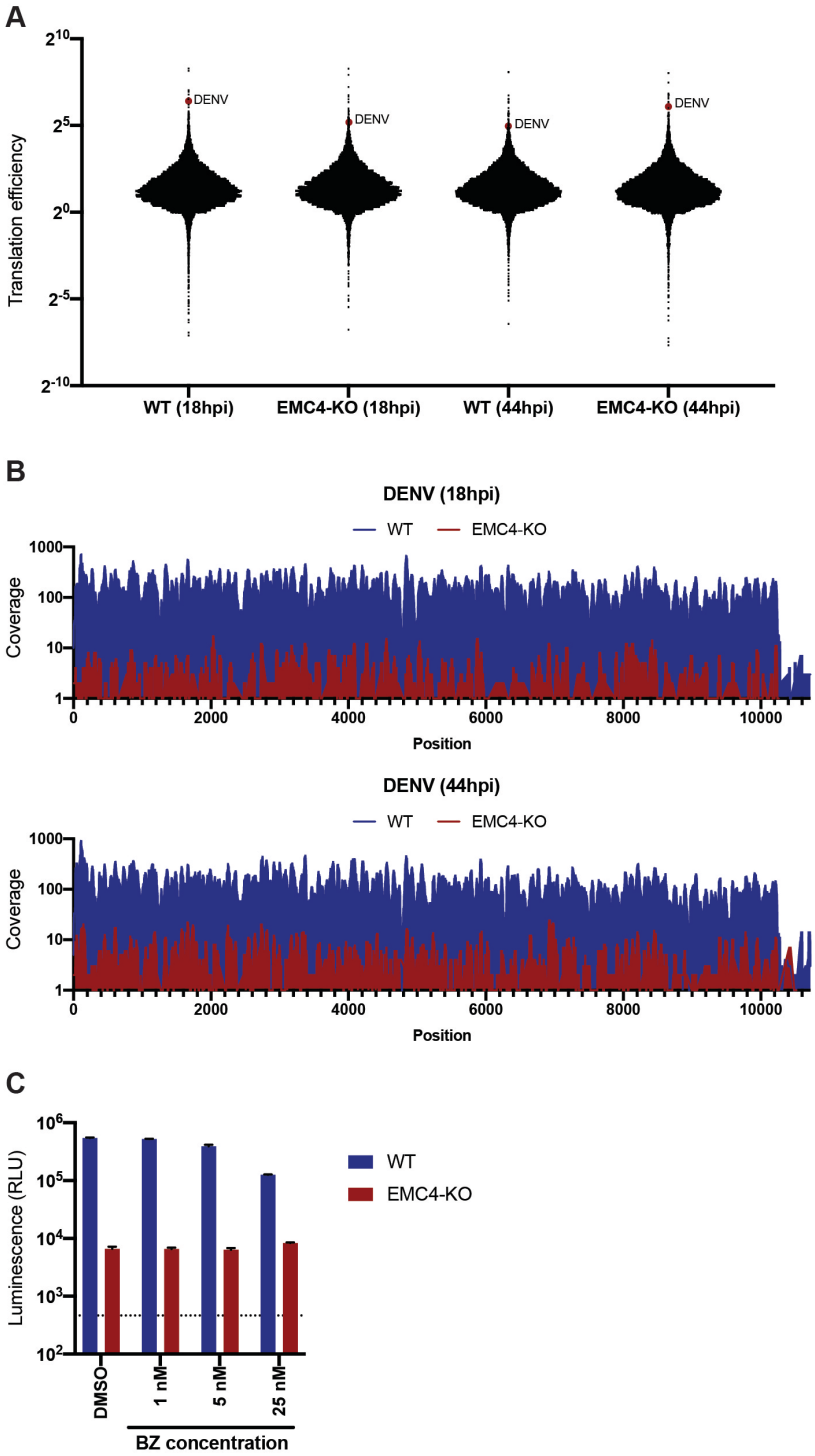

Figure S3: EMC knockout does not largely affect viral translation efficiency but leads to post-translational protein degradation

449 (A) Translation efficiencies of cellular and DENV mRNA in WT and EMC4-KO cells at 18 and
450 44hpi. DENV is highlighted as red dot.
451 (B) Footprint distribution of Ribo-seq reads mapped to the DENV genome in WT and EMC4-KO
452 cells at 18 and 44hpi. Nucleotide position of DENV genome is indicated on x-axis.
453 (C) DENV-Luc infection of WT and EMC4 KO HEK293FT cells treated with DMSO control or
454 different concentrations of BZ for 24h. Dotted line indicates background signal from uninfected
455 cells.

Figure S4

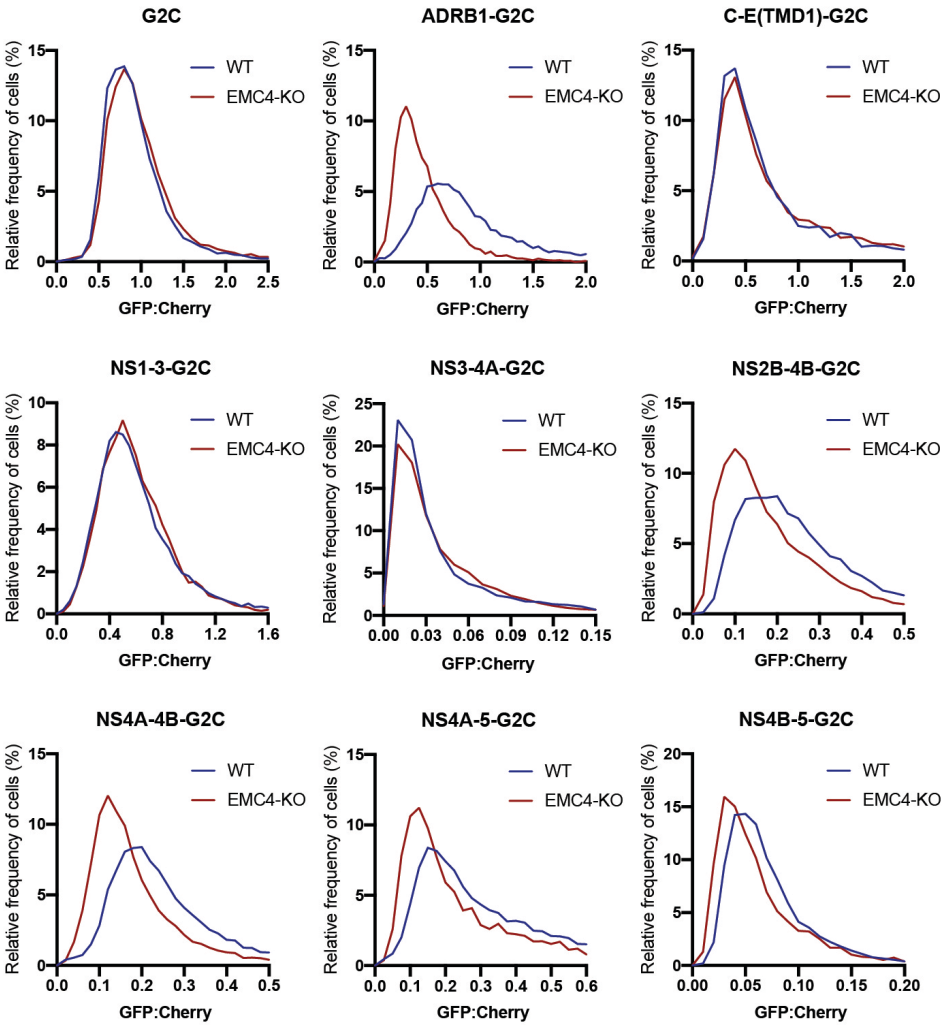

Figure S4: EMC is required for proper biogenesis of the NS4A-NS4B region of the DENV polyprotein

Flow cytometry measurements of GFP:mCherry fluorescence ratio for G2C constructs in WT and EMC4-KO HEK293FT cells. The fluorescence ratios are depicted as histograms. ADRB1=β_1-adrenergic receptor.

Figure S5

Virus isolate	Position	nt change	Coverage	Variant frequency	Reference frequency	aa change
EMC adapted DENV #3	226	T -> C	9754	99.80%	0.10%	synonymous
EMC adapted DENV #1	725	T -> C	5653	99.70%	0.10%	Val->Ala
EMC adapted DENV #1	1531	C -> T	3686	98.40%	0.80%	synonymous
EMC adapted DENV #2	1531	C -> T	9399	99.90%	0.10%	synonymous
EMC adapted DENV #3	1531	C -> T	14698	99.50%	0.20%	synonymous
EMC adapted DENV #1	1818	C -> A	3366	99.00%	0.20%	synonymous
EMC adapted DENV #3	4018	C -> T	16149	94.50%	5.50%	synonymous
EMC adapted DENV #2	5493	A -> G	10626	99.00%	0.50%	synonymous
EMC adapted DENV #1	6665	A -> G	3172	99.70%	0.10%	Tyr->Cys
EMC adapted DENV #2	6665	A -> G	8932	99.40%	0.50%	Tyr->Cys
EMC adapted DENV #3	6665	A -> G	13319	99.50%	0.20%	Tyr->Cys
EMC adapted DENV #1	7558	A -> T	4205	98.40%	0.40%	Asn->Tyr
EMC adapted DENV #2	7558	A -> T	10497	99.40%	0.10%	Asn->Tyr
EMC adapted DENV #3	7558	A -> T	16401	99.00%	0.04%	Asn->Tyr
EMC adapted DENV #3	7581	C -> T	16867	94.20%	5.70%	synonymous
EMC adapted DENV #3	8546	G -> A	15538	94.80%	5.10%	Arg->Lys

Figure S5: Adaptation of DENV to EMC-KO cells reveals conserved point mutations in NS4A and NS4B

Table containing all identified SNPs from the three isolated EMC-adapted viruses. A minimum variant frequency cutoff of 80% was used.

471 **Material and methods**

472 ***Cell culture and viruses***

473 Huh7.5.1 (gift from Frank Chisari) and HEK293FT (Thermo Scientific) were cultured in DMEM
474 (Gibco) supplemented with 10% fetal bovine serum (Omega Scientific), penicillin/streptomycin
475 (Gibco), non-essential amino acids (Gibco) and L-glutamine (Gibco) at 37C and 5% CO_2. Parental
476 cell lines were tested negative for mycoplasma. The following virus strains were used: DENV
477 serotype 2 strain 16681 (stocks kindly provided by Caleb Marceau), DENV-Luc (stocks kindly
478 provided by Jan Carette) (Marceau et al., 2016), WNV Kunjin strain CH16532 (stocks kindly
479 provided by Jan Carette), ZIKV PRVABC59 (stocks kindly provided by Jan Carette) and HCV
480 JFH1 (stocks kindly provided by Jan Carette). Viral titers were determined by plaque- or focus-
481 forming assay.

482

483 ***Chemical compounds***

484 MK-0608 (2'-C-Methylcytidine) was purchased from Carbosynth and used at a concentration of
485 25 µM. Bortezomib was obtained from Selleckchem and used at concentrations 1-50 nM. For all
486 experiments, DMSO controls were included. Cycloheximide was purchased from Sigma and used
487 at 100 µg/ml for ribosome profiling experiments.

488

489 ***Generation of knockout cell lines***

490 Oligos containing sgRNA sequence were annealed and ligated into pX458 (gift from Feng Zhang;
491 Addgene plasmid # 48138). Cells were transfected with pX458 using Lipofectamine 3000
492 (Invitrogen) and two days later GFP positive cells were single-cell sorted into 96-well plates using
493 a Sony SH800 cell sorter. For genotyping, genomic DNA was isolated from obtained clones using
494 QuickExtract (Lucigen), the sgRNA-targeted sites PCR amplified and the products Sanger-
495 sequenced. Obtained sequences were compared to reference sequences for indel mutations. In
496 the case of heterozygous mutations, TIDE was used to deconvolute sequencing traces (Brinkman

497 et al., 2014). A list of all used sgRNA oligo and genotyping primer sequences can be found in
498 Supplementary Table 2.
499
500 ***Dengue Luciferase assay***
501 Huh7.5.1 or HEK293FT cells were seeded in 96-well plates and infected with DENV-Luc at an
502 moi of 0.01. Cells were harvested in Renilla Lysis buffer and luminescence was measured using
503 Renilla Luciferase Assay system (Promega) on a Spectramax i3x Multi-Mode Microplate Reader
504 (Molecular Devices).
505
506 ***Quantitative RT-PCR***
507 Huh7.5.1 or HEK293FT cells were plated in 96-well plates (in triplicates for each condition) and
508 infected with an moi of 0.5 for all viruses. Cells were then harvested at 30hpi for ZIKV, 48hpi for
509 DENV and WNV, and 72hpi for HCV using the Power SYBR Cells-to-CT kit (Invitrogen). After
510 reverse transcription, quantitative PCR was performed on a Bio-Rad CFX96 Touch system. All
511 viral RNA levels were normalized to 18S levels. For viral internalization assay, 96-well plates
512 containing WT or EMC4 KO Huh7.5.1 cells were put on ice before infection with DENV at an moi
513 of 30. Cells were incubated for 1h before moving them to a 37C incubator. At each harvest
514 timepoint, cells were washed three times with PBS and lysed as described above. All qPCR primer
515 sequences can be found in Supplementary Table 2.
516
517 ***Lentiviral complementation***
518 EMC2 (GenScript; clone OHu30604) and EMC4 cDNA (GenScript; clone OHu00964) were PCR
519 amplified using tgtggtggaattctgcagataccATGGCGAAGGTCTCAGA /
520 CGGCCGCCACTGTGCTGGATTTACTTATCGTCGTCATCCTTGTAATCAGACTGGGTGATC
521 and tgtggtggaattctgcagataccATGACGGCCCAGGGG /
522 CGGCCGCCACTGTGCTGGATTTACTTATCGTCGTCATCCTTGTAATCCAAAAGCAGTCCT,

523 respectively, and cloned into EcoRV-cut pLenti CMV Puro DEST (w118-1) (gift from Eric
524 Campeau & Paul Kaufman; Addgene plasmid # 17452) using NEBuilder® HiFi DNA Assembly
525 Master Mix (New England BioLabs). Lentivirus was produced in HEK293FT, respective KO cells
526 transduced with filtered, lentiviral containing supernatant and selected using 2-4 µg/ml puromycin
527 (Gibco) for 3-4 days.
528
529 ***Replicon assay***
530 DENV replicon plasmid (Marceau et al., 2016) was linearized using XbaI restriction enzyme.
531 Replicon RNA was generated using the MEGAscript T7 Kit (Invitrogen) with the reaction
532 containing 5mM m7G(5')ppp(5')G RNA Cap Structure Analog (New England BioLabs). Resulting
533 RNA was purified by lithium chloride precipitation. For electroporation, 2 million WT or EMC4 KO
534 HEK293FT cells were washed twice in PBS, resuspended in 100 µl SF Nucleofector solution
535 (Lonza), mixed with 4 µg replicon RNA, transferred to a 100ul nucleocuvette and pulsed using
536 program CM-130 on an Amaxa 4D-Nucleofector™ X Unit (Lonza). Cells were then resuspended
537 in antibiotic-free medium, distributed into 96-wells and lysed at different timepoints post-
538 electroporation using Renilla Lysis buffer. Luminescence was measured using Renilla Luciferase
539 Assay system (Promega) on a Spectramax i3x Multi-Mode Microplate Reader (Molecular
540 Devices).
541
542 ***Immunoblotting***
543 Cell were lysed using Laemmli SDS sample buffer containing 5% beta-mercaptoethanol and
544 boiled for 10min. Lysates were separated by SDS-PAGE on pre-cast Bio-Rad 4-15% poly-
545 acrylamide gels in Bio-Rad Mini-Protean electrophoresis system. Proteins were transferred onto
546 PVDF membranes using Bio-Rad Trans-Blot Turbo transfer system. PVDF membranes were
547 blocked with PBS buffer containing 0.1% Tween-20 and 5% non-fat milk. Blocked membranes
548 were incubated with primary antibody diluted in blocking buffer and incubated overnight at 4C on

549 a shaker. Primary antibodies were detected by incubating membranes with 1:10000 dilution of
550 HRP-conjugated (Southern Biotech) or IRDye-conjugated (LI-COR) secondary anti-mouse and
551 anti-rabbit antibodies for 1 h at room temperature. Blots were visualized using a ChemiDoc™ MP
552 Imaging System (Bio-Rad). The following primary antibodies (and their dilutions) were used in
553 this study: p84 (Genetex, GTX70220) at 1:2000, GAPDH (SCBT, sc-32233) at 1:2000,
554 EMC2/TTC35 (Proteintech, 25443-1-AP) at 1:750, EMC4 (Bethyl, A305-752A) at 1:500, Dengue
555 virus prM protein (Genetex, GTX128093) at 1:1000, Dengue virus Capsid protein (Genetex,
556 GTX103343) at 1:1000, Dengue virus NS2B (Genetex, GTX124246) at 1:1000, Dengue virus NS3
557 protein (Genetex, GTX629477) at 1:1000, Dengue virus NS4B protein (Genetex, GTX124250) at
558 1:1000, Dengue virus Type 2 NS5 protein (Genetex, GTX629447) and GFP (Genetex,
559 GTX113617) at 1:5000.
560
561 ***Ribosome profiling***
562 WT and EMC4 KO HEK293FT were plated in 10cm dishes and infected with DENV at an of 100
563 for the 18hpi harvest and an moi of 0.5 for the 44hpi harvest. Cells were treated with 100 µg/ml
564 cycloheximide for 2 min, washed once with polysome gradient buffer (20 mM Tris pH 7.5, 150
565 mM NaCl, 5 mM $MgCl_2$, 100 µg/mL cycloheximide, 1 mM DTT) and then lysed using 500 µl of
566 polysome lysis buffer (20 mM Tris pH 7.5, 150 mM NaCl, 5 $MgCl_2$, 1% Triton X-100, 1 mM DTT,
567 100 µg/mL cycloheximide, 24 U/ml Turbo DNase (Ambion)) per plate. Cells/lysates were collected
568 using cell scrapers and incubated on ice for 15min. Crude lysates were centrifuged at 20,000 x g
569 for 2 min at 4C and the cleared polysome-containing lysates flash frozen by immersion in liquid
570 nitrogen and stored at -80C until further processing. For ribosomal footprinting, 30 µg total RNA
571 diluted in polysome buffer to a total volume of 200ul were treated with 750 U/ml RNaseI (Ambion)
572 for 45min at 25C with shaking (300rpm). RNase activity was quenched by adding 10ul
573 SuperaseIN (Invitrogen) and placing samples on ice. Note that 10% of the lysates were saved for
574 RNA-seq library preparation (see below). A 1ml sucrose cushion was added to the bottom of a

575 13mm x 56mm thick-wall polycarbonate tube (Beckman Coulter) for each sample and the footprint
576 digests were layered on top. Tubes were ultracentrifuged at 100,000 rpm for 4h at 4C in a
577 TLA100.3 rotor (Beckman Coulter). After spin, supernatant was removed and the monosome-
578 containing pellet was resuspended in 300 µl Trizol LS (Life Technologies) for RNA extraction
579 using the Direct-Zol kit (Zymo). Ribo-seq NGS libraries of ribosomal footprints were generated as
580 previously described (Shurtleff et al., 2018).
581 For corresponding RNA-seq libraries RNA was extracted from the remaining undigested cleared
582 lysates using Trizol and the Direct-Zol kit. 1 µg purified total RNA was used as input for the Truseq
583 stranded total RNA Gold library prep (Illumina). Ribosomal RNA was depleted using Ribo-Zero
584 H/M/R Gold and depleted RNA fragmented for 8min at 94C. Following first and second strand
585 synthesis products were purified using SPRI beads. KAPA dual-indexed adapters (Kapa
586 Biosystems, KK8722) were used for adapter ligation. Finally, PCR enriched products were
587 cleaned up using SPRI. Ribo-seq and RNA-seq libraries were analyzed on Bioanalyzer or
588 TapeStation (Agilent) before sequencing on a NextSeq 500 platform (Illumina) in separate runs
589 with 400M read output.
590
591 ***Analysis of ribosome profiling data***
592 Reads from Ribo-seq or RNA-seq were preprocessed by removing low-quality reads and trimming
593 of adaptor sequences. Next, ribosomal RNA reads were removed using Bowtie. Remaining reads
594 were aligned to the human reference genome file also containing the genomic DENV2 16681
595 sequence using Tophat to generate read count tables with RPKMs for each transcript. A cutoff of
596 at least 5 RPKMs was used for further analysis of transcripts/footprint counts and $\log_2$ fold-change
597 (FC) was calculated between corresponding EMC4 KO and WT samples for both Ribo-seq and
598 RNA-seq. To calculate translation efficiency (TE), the FC in Ribo-seq RPKMs was normalized by
599 the FC in RNA-seq RPKMs for each transcript.

600 To analyze the footprint distribution of Ribo-seq reads across the DENV genome, DENV specific
601 reads were mapped to the DENV2 16681 reference sequence using Geneious Prime and
602 coverage at each nucleotide position was determined.
603
604 ***Dual fluorescence cytometry assay***
605 eGFP was amplified from pX458 with adding overhang to plenti-CMV-Puro (EcoRV cut site), a
606 Kozak sequence and ATG start codon for the G2C-only construct or with an additional overhang
607 to GlySer-linker sequence for fusion with DENV fragments. T2A-mCherry was amplified from
608 pX458 where eGFP had been replaced with mCherry. Different regions of the DENV genome
609 were amplified from the DENV2 16681 infectious clone plasmid (gift from Karla Kirkegaard) with
610 addition of overhang sequences to plenti-CMV backbone, Kozak sequence and ATG start codon
611 on 5'end and to GlySer-linker-GFP fragment on 3'end. ADRB1 was amplified from pcDNA3 Flag
612 beta-1-adrenergic-receptor (gift from Robert Lefkowitz; Addgene plasmid # 14698). All fragments
613 contained ~20bp overhangs and were assembled into EcoRV cut pLenti CMV Puro DEST (w118-
614 1) using NEBuilder® HiFi DNA Assembly Master Mix (New England BioLabs) or Gibson-like
615 master mix (Berkeley MacroLabs) to generate G2C reporter expression constructs. All constructs
616 were verified by Sanger sequencing. Primer sequences can be found in Supplementary Table 2.
617 For the G2C dual fluorescence assay, cells were seeded in 24- or 12-well plates and transfected
618 with G2C constructs using Lipofectamine 3000 (Invitrogen). 24-48h later cells were trypsinized,
619 filtered (70µm), and analyzed by flow cytometry using a Cytoflex S flow cytometer (Beckman
620 Coulter). At least 5,000 and 10,000 mCherry positive cells were recorded for Huh7.5.1 and
621 HEK293FT, respectively. For analysis, cells were gated based on FSC/SSC, FSC-H/FSC-A
622 (singlets) and finally ECD (mCherry) and FITC (eGFP) using FlowJo 10. Raw fluorescence data
623 for all gated fluorescent cells was exported and the eGFP:mCherry intensity ratios were calculated
624 for individual cells. All fluorescence ratios were normalized to the mean of the G2C-only construct.
625 Distributions of fluorescence ratios were plotted as histograms using GraphPad Prism 8.

626

627 ***Viral adaptation***

628 WT DENV serotype 2 strain 16681 was serially passaged every 3-4 days onto newly plated EMC4
629 KO Huh7.5.1 cells by transferring increasingly diluted supernatant from infected cells (starting at
630 2-fold dilutions for the first 3 passages, then stepwise increase of dilutions to 100-fold for the final
631 passages). Six independent passaging experiments were started and cytopathic effects were
632 observed in three of the replicates after approximately 20-22 passages. Supernatant was then
633 harvested, filtered through a 0.45 um filter to remove cellular debris, and RNA was extracted using
634 Trizol LS and Direct-Zol kit (Zymo). Additionally, RNA was extracted from WT DENV stock. To
635 prepare sequencing libraries, Truseq stranded total RNA Gold library kit (Illumina) was used.
636 Isolated RNA was fragmented for 4min at 94C without prior Ribo-Zero depletion, followed by first
637 and second strand synthesis, and adapter ligation. Fragments were amplified in presence of
638 SYBR Green on Bio-Rad CFX96 and reaction was stopped for each sample before it reached
639 plateau (~20-24 cycles). Libraries from different virus isolates were pooled and sequenced on
640 iSeq 100 (Illumina) with 2x75bp reads.

641 For analysis, Geneious Prime was used: Fastq files were imported as paired reads and Truseq
642 adapters and low-quality sequences (minimum 20) were trimmed using BBDuk. Next, reads were
643 mapped to the WT 16681 reference genome using the Geneious Mapper at medium-low
644 sensitivity and with 5 iterations for fine-tuning. All samples had a minimum coverage of 1000 at
645 all nucleotide positions. Finally, SNPs between adapted and WT stock viruses were called with a
646 minimum variance frequency of 80%. To compare acquired non-synonymous point mutations to
647 a large dataset of sequenced DENV2 strains, 1,359 complete genome sequences from NCBI
648 were mapped to the DENV2 16681 strain containing adapted mutations.

649

650 ***Generation of EMC adapted DENV-Luciferase***

651 DENV-Luc infectious clone containing adapted mutations were generated by PCR amplification
652 from WT DENV-Luc infectious clone plasmid (gift from Jan Carette). For DENV-Luc(A6665G)
653 fragments were amplified using GAAGAGTGATGGTTATGGTAGGC /
654 CTGTATTTGTGCGCACCATAGGAGGATG and CATCCTCCTATGGTGCGCACAAATACAG /
655 GTGATCTTCATTTAAGAATCCTAGGGCTTC. For DENV-Luc(A7558T) fragments were
656 amplified using GAAGAGTGATGGTTATGGTAGGC / CCCCTTCTTGTGTAGGTTGTGTTCTTC
657 and GAAGAACACAACCTACACAAGAAGGGG / GTGATCTTCATTTAAGAATCCTAGGGCTTC.
658 For DENV-Luc(A6665G, A7558T) fragments were amplified using
659 GAAGAGTGATGGTTATGGTAGGC / CTGTATTTGTGCGCACCATAGGAGGATG,
660 CATCCTCCTATGGTGCGCACAAATACAG / CCCCTTCTTGTGTAGGTTGTGTTCTTC, and
661 GAAGAACACAACCTACACAAGAAGGGG / GTGATCTTCATTTAAGAATCCTAGGGCTTC.
662 PCR products were cloned into NarI and AvrII cut WT DENV-Luc infectious clone using
663 NEBuilder® HiFi DNA Assembly Master Mix (New England BioLabs) and transformed into Stbl3
664 bacteria (Berkeley MacroLabs). Constructs were verified by Sanger sequencing. Plasmids were
665 linearized with XbaI and RNA was generated by in-vitro transcription using the MEGAscript T7 Kit
666 (Invitrogen) with the reaction containing 5mM m7G(5')ppp(5')G RNA Cap Structure Analog (New
667 England BioLabs). Resulting RNA was purified by lithium chloride precipitation and transfected
668 into BHK-21 cells using Lipofectamine 3000 for viral production. Supernatants were harvested 6-
669 9 days post-transfection.
670
671 ***Co-immunoprecipitation***
672 HEK293FT EMC4 KO cells complemented with FLAG-tagged EMC4 were seeded in a 10cm dish
673 and infected with DENV for 96h. Cells were washed with PBS and then collected in 1ml Pierce
674 RIPA buffer (Thermo Scientific) containing 1mM PMSF (Thermo Scientific), 5mM EDTA and 1x
675 Halt Protease Inhibitor Cocktail (Thermo Scientific) with help of cell scrapers. Cells were lysed on
676 ice for 1h with occasional vortexing and subsequently centrifuged at 15,000 x g for 10min at 4C

677 to clear lysates. For co-immunoprecipitation, clarified lysates were incubated at 4C overnight with
678 Anti-FLAG® M2 Magnetic Beads (Sigma) while rotating. Beads were washed three times using
679 TBS-T and eluted by boiling in 2x Laemmli buffer. Eluates were loaded for SDS-PAGE and stained
680 for viral proteins.
681
682 ***Statistical analysis***
683 GraphPad Prism 8 was used to analyze data and perform statistical tests. Unpaired *t*-tests were
684 applied to measure statistical significance of differences in DENV infection between WT and EMC
685 KO cells.
686
687 **Supplementary tables**
688 ***Supplementary_Table_1***
689 Ribosome profiling data including read counts and fold change for Ribo-seq and RNA-seq used
690 to generate Figures 3A-C.
691
692 ***Supplementary_Table_2***
693 Table of oligos used in this study: sgRNA oligos, genotyping primers, qPCR primers, primers to
694 generate G2C constructs
695
696

697 **References**

698 Abernathy, E., Mateo, R., Majzoub, K., van Buuren, N., Bird, S.W., Carette, J.E., and
699 Kirkegaard, K. (2019). Differential and convergent utilization of autophagy components by
700 positive-strand RNA viruses. PLoS Biol. *17*, e2006926.

701 Beaucourt, S., and Vignuzzi, M. (2014). Ribavirin: a drug active against many viruses with
702 multiple effects on virus replication and propagation. Molecular basis of ribavirin resistance.
703 Curr. Opin. Virol. *8*, 10–15.

704 Brinkman, E.K., Chen, T., Amendola, M., and van Steensel, B. (2014). Easy quantitative
705 assessment of genome editing by sequence trace decomposition. Nucleic Acids Res. *42*, e168–
706 e168.

707 Chen, Y.-L., Yokokawa, F., and Shi, P.-Y. (2015). The search for nucleoside/nucleotide analog
708 inhibitors of dengue virus. Antiviral Res. *122*, 12–19.

709 Chitwood, P.J., and Hegde, R.S. (2019). The Role of EMC during Membrane Protein
710 Biogenesis. Trends Cell Biol.

711 Chitwood, P.J., Juszkiewicz, S., Guna, A., Shao, S., and Hegde, R.S. (2018). EMC Is Required
712 to Initiate Accurate Membrane Protein Topogenesis. Cell *175*, 1507-1519.e16.

713 Christianson, J.C., Olzmann, J.A., Shaler, T.A., Sowa, M.E., Bennett, E.J., Richter, C.M., Tyler,
714 R.E., Greenblatt, E.J., Harper, J.W., and Kopito, R.R. (2011). Defining human ERAD networks
715 through an integrative mapping strategy. Nat. Cell Biol. *14*, 93–105.

716 Coelho, J.P.L., Stahl, M., Bloemeke, N., Meighen-Berger, K., Alvira, C.P., Zhang, Z.-R., Sieber,
717 S.A., and Feige, M.J. (2019). A network of chaperones prevents and detects failures in
718 membrane protein lipid bilayer integration. Nat. Commun. *10*.

719 Guna, A., Volkmar, N., Christianson, J.C., and Hegde, R.S. (2018). The ER membrane protein
720 complex is a transmembrane domain insertase. Science *359*, 470–473.

721 Ingolia, N.T., Ghaemmaghami, S., Newman, J.R.S., and Weissman, J.S. (2009). Genome-Wide
722 Analysis in Vivo of Translation with Nucleotide Resolution Using Ribosome Profiling. Science
723 *324*, 218–223.

724 Jonikas, M.C., Collins, S.R., Denic, V., Oh, E., Quan, E.M., Schmid, V., Weibezahn, J.,
725 Schwappach, B., Walter, P., Weissman, J.S., et al. (2009). Comprehensive characterization of
726 genes required for protein folding in the endoplasmic reticulum. Science *323*, 1693–1697.

727 Krishnan, M.N., Ng, A., Sukumaran, B., Gilfoy, F.D., Uchil, P.D., Sultana, H., Brass, A.L.,
728 Adametz, R., Tsui, M., Qian, F., et al. (2008). RNA interference screen for human genes
729 associated with West Nile virus infection. Nature *455*, 242–245.

730 Lee, Y.-R., Kuo, S.-H., Lin, C.-Y., Fu, P.-J., Lin, Y.-S., Yeh, T.-M., and Liu, H.-S. (2018). Dengue
731 virus-induced ER stress is required for autophagy activation, viral replication, and pathogenesis
732 both in vitro and in vivo. Sci. Rep. *8*, 489.

733 Lin, C., Amberg, S.M., Chambers, T.J., and Rice, C.M. (1993). Cleavage at a novel site in the
734 NS4A region by the yellow fever virus NS2B-3 proteinase is a prerequisite for processing at the
735 downstream 4A/4B signalase site. J. Virol. *67*, 2327–2335.

736 Ma, H., Dang, Y., Wu, Y., Jia, G., Anaya, E., Zhang, J., Abraham, S., Choi, J.-G., Shi, G., Qi, L.,
737 et al. (2015). A CRISPR-Based Screen Identifies Genes Essential for West-Nile-Virus-Induced
738 Cell Death. Cell Rep. *12*, 673–683.

739 Marceau, C.D., Puschnik, A.S., Majzoub, K., Ooi, Y.S., Brewer, S.M., Fuchs, G., Swaminathan,
740 K., Mata, M.A., Elias, J.E., Sarnow, P., et al. (2016). Genetic dissection of Flaviviridae host
741 factors through genome-scale CRISPR screens. Nature *535*, 159–163.

742 Miller, S., Sparacio, S., and Bartenschlager, R. (2006). Subcellular Localization and Membrane
743 Topology of the Dengue Virus Type 2 Non-structural Protein 4B. J. Biol. Chem. *281*, 8854–
744 8863.

745 Miller, S., Kastner, S., Krijnse-Locker, J., Bühler, S., and Bartenschlager, R. (2007). The Non-
746 structural Protein 4A of Dengue Virus Is an Integral Membrane Protein Inducing Membrane
747 Alterations in a 2K-regulated Manner. J. Biol. Chem. *282*, 8873–8882.

748 Muñoz-Jordán, J.L., Laurent-Rolle, M., Ashour, J., Martínez-Sobrido, L., Ashok, M., Lipkin, W.I.,
749 and García-Sastre, A. (2005). Inhibition of alpha/beta interferon signaling by the NS4B protein of
750 flaviviruses. J. Virol. *79*, 8004–8013.

751 Neufeldt, C.J., Cortese, M., Acosta, E.G., and Bartenschlager, R. (2018). Rewiring cellular
752 networks by members of the Flaviviridae family. Nat. Rev. Microbiol. *16*, 125–142.

753 Peña, J., and Harris, E. (2011). Dengue virus modulates the unfolded protein response in a
754 time-dependent manner. J. Biol. Chem. *286*, 14226–14236.

755 Puschnik, A.S., Marceau, C.D., Ooi, Y.S., Majzoub, K., Rinis, N., Contessa, J.N., and Carette,
756 J.E. (2017). A Small-Molecule Oligosaccharyltransferase Inhibitor with Pan-flaviviral Activity.
757 Cell Rep. *21*, 3032–3039.

758 Reid, D.W., Campos, R.K., Child, J.R., Zheng, T., Chan, K.W.K., Bradrick, S.S., Vasudevan,
759 S.G., Garcia-Blanco, M.A., and Nicchitta, C.V. (2018). Dengue Virus Selectively Annexes
760 Endoplasmic Reticulum-Associated Translation Machinery as a Strategy for Co-opting Host Cell
761 Protein Synthesis. J. Virol. *92*, e01766-17.

762 Roosendaal, J., Westaway, E.G., Khromykh, A., and Mackenzie, J.M. (2006). Regulated
763 cleavages at the West Nile virus NS4A-2K-NS4B junctions play a major role in rearranging
764 cytoplasmic membranes and Golgi trafficking of the NS4A protein. J. Virol. *80*, 4623–4632.

765 Savidis, G., McDougall, W.M., Meraner, P., Perreira, J.M., Portmann, J.M., Trincucci, G., John,
766 S.P., Aker, A.M., Renzette, N., Robbins, D.R., et al. (2016). Identification of Zika Virus and
767 Dengue Virus Dependency Factors using Functional Genomics. Cell Rep. *16*, 232–246.

768 Senft, D., and Ronai, Z.A. (2015). UPR, autophagy, and mitochondria crosstalk underlies the
769 ER stress response. Trends Biochem. Sci. *40*, 141–148.

770 Sessions, O.M., Barrows, N.J., Souza-Neto, J.A., Robinson, T.J., Hershey, C.L., Rodgers, M.A.,
771 Ramirez, J.L., Dimopoulos, G., Yang, P.L., Pearson, J.L., et al. (2009). Discovery of insect and
772 human dengue virus host factors. Nature *458*, 1047–1050.

773 Shao, S., and Hegde, R.S. (2011). Membrane Protein Insertion at the Endoplasmic Reticulum.
774 Annu. Rev. Cell Dev. Biol. *27*, 25–56.

775 Shurtleff, M.J., Itzhak, D.N., Hussmann, J.A., Oakdale, N.T.S., Costa, E.A., Jonikas, M.,
776 Weibezahn, J., Popova, K.D., Jan, C.H., Sinitcyn, P., et al. (2018). The ER membrane protein
777 complex interacts cotranslationally to enable biogenesis of multipass membrane proteins. ELife
778 *7*, e37018.

779 Su, H.-L., Liao, C.-L., and Lin, Y.-L. (2002). Japanese Encephalitis Virus Infection Initiates
780 Endoplasmic Reticulum Stress and an Unfolded Protein Response. J. Virol. *76*, 4162–4171.

781 Volkmar, N., Thezenas, M.-L., Louie, S.M., Juszkiewicz, S., Nomura, D.K., Hegde, R.S.,
782 Kessler, B.M., and Christianson, J.C. (2019). The ER membrane protein complex promotes
783 biogenesis of sterol-related enzymes maintaining cholesterol homeostasis. J. Cell Sci. *132*.

784 Zhang, R., Miner, J.J., Gorman, M.J., Rausch, K., Ramage, H., White, J.P., Zuiani, A., Zhang,
785 P., Fernandez, E., Zhang, Q., et al. (2016). A CRISPR screen defines a signal peptide
786 processing pathway required by flaviviruses. Nature *535*, 164–168.

787 Zou, J., Lee, L.T., Wang, Q.Y., Xie, X., Lu, S., Yau, Y.H., Yuan, Z., Geifman Shochat, S., Kang,
788 C., Lescar, J., et al. (2015). Mapping the Interactions between the NS4B and NS3 proteins of
789 dengue virus. J. Virol. *89*, 3471–3483.

790